Acta Geotechnica
https://doi.org/10.1007/s11440-024-02387-9

RESEARCH PAPER

DEM investigation into the small-strain stiffness of bio-cemented soils

Aoxi Zhang[1] · Vanessa Magnanimo[2] · Hongyang Cheng[2] · Timo J. Heimovaara[1] · Anne-Catherine Dieudonné[1]

Received: 15 October 2023 / Accepted: 18 August 2024

Abstract
Bio-mediated methods, such as microbially induced carbonate precipitation, are promising techniques for soil stabilisation. However, uncertainty about the spatial distribution of the minerals formed and the mechanical improvements impedes bio-mediated methods from being translated widely into practice. To bolster confidence in bio-treatment, non-destructive characterisation is desired. Seismic methods offer the possibility to monitor the effectiveness and mechanical efficiency of bio-treatment both in the laboratory and in the field. To aid the interpretation of shear wave velocity measurements, this study uses the discrete element method to examine the small-strain stiffness of bio-cemented sands. Bio-cemented specimens with different characteristics, including properties of the host sand (void ratio, uniformity of particle size distribution) and properties of the precipitated minerals (distribution pattern, content, Young's modulus), are modelled and subjected to static probing. The mechanisms affecting the small-strain properties of cemented soils are investigated from microscopic observations. The results identify two mechanisms controlling the mechanical reinforcement associated with bio-cementation, namely the number of effective bonds and the ability of a single bond to improve stiffness. The results show that the dominant mechanism varies with the properties of the host sand. These results support the use of seismic measurements to assess the mechanical efficiency and effectiveness of bio-mediated treatment.

Keywords Bio-cemented soils · Discrete element modelling · Microstructure · Small-strain stiffness

1 Introduction

Bio-mediated soil improvement methods have attracted increasing attention in civil engineering over the past two decades [13, 22, 24, 37, 56, 62, 68]. Prominent techniques include microbially induced carbonate precipitation (MICP) and enzyme induced carbonate precipitation (EICP). These methods rely on geochemical reactions to drive the precipitation of calcium carbonate, which can act as cementing agent and bond soil grains. As a result, MICP and EICP are able to improve the mechanical properties of soils and can be applied for soil stabilisation (see [9, 12, 35, 47, 66, 69, 71, 77] among others).

Despite the promising applications of bio-mediated methods, critical challenges have impeded bio-mediated methods from being translated into practice at an industrial scale. A widely recognised challenge is the uncertainty of bio-mediated treatment [29, 38, 47, 67]. Due to the intrinsic heterogeneous nature of the subsurface, obtaining a uniform treatment in the field proves difficult, and the spatial distribution of the precipitated carbonate crystals is affected by significant uncertainty. Furthermore, laboratory studies have shown that the distribution pattern of carbonate crystals within the pore space of soils can vary significantly. These uncertainties are found to lead to large variations in the mechanical performance of bio-cemented soils. Figure 1 shows that, for a given carbonate content, the mechanical performance of bio-cemented soils can vary within a wide range. This variability can be attributed to differences in the treated sand properties (e.g. particle size distribution, initial void ratio) and treatment protocol (e.g. urease activity and cementation solution), among others. However, intrinsic variability of the results is also observed, for the same material treated following the same protocol. These uncertainties can hinder the practical

✉ Anne-Catherine Dieudonné
A.A.M.Dieudonne@tudelft.nl

[1] Department of Geoscience and Engineering, Delft University of Technology, Delft, The Netherlands

[2] Department of Civil Engineering and Management, University of Twente, Enschede, The Netherlands

Published online: 18 September 2024

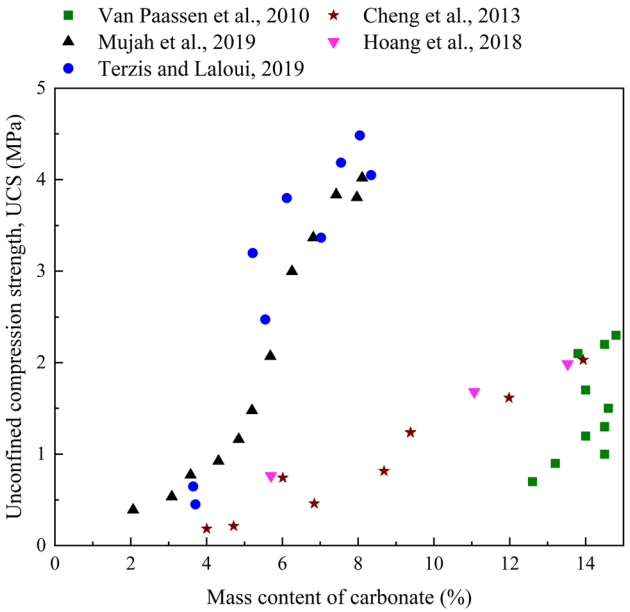

Fig. 1 Variability in the mechanical performance of bio-cemented soils. Experimental results of unconfined compression strength tests as a function of carbonate mass content

implementation of bio-mediated methods. Therefore, it is important to increase confidence in the effectiveness and mechanical efficiency of bio-treatment methods.

To ascertain the improvement of bio-mediated treatment, measurements such as mechanical tests (e.g. uniaxial or triaxial tests), acid washing and micro-computed tomography scans can be used to quantify the mechanical improvements and mass content of the precipitated carbonate. However, these measurements are destructive and costly. Moreover, the measured quantities only provide information on the local mechanical efficiency and effectiveness of the treatment. Therefore, non-destructive characterisation methods that are easy to implement on-site at a large scale are much preferred.

Seismic monitoring is often an effective tool in geotechnical engineering [51, 61, 72]. It can provide real-time and non-destructive monitoring of the wave signals of the subsurface. Seismic measurements rely on detecting and recording wave signals resulting from an artificial source and travelling through the subsurface. The wave velocity (e.g. shear wave velocity) can be derived from the collected data. The derived wave velocity is often used for process monitoring throughout bio-treatment [13, 41, 47, 52]. However, the information behind the shear wave velocity remains poorly understood. Specifically, what factors affect the measured shear wave velocity and how to interpret the measured shear wave velocity of bio-treated soil are still to be investigated.

This study contributes to the interpretation of the obtained shear wave velocity in laboratory tests, which supports shear wave measurement to assess the mechanical efficiency and effectiveness of bio-mediated treatment. Fundamental insights on the effect of bio-cementation on the shear wave velocity of bio-cemented soils are provided in an indirect way, i.e. by examining the small-strain stiffness (G_0) of bio-cemented soils instead of directly measuring the shear wave velocity (V_s).

2 Factors affecting G_0 of bio-cemented soil

Potential factors that may affect the small-strain stiffness of bio-cemented soil could be the properties of the host soil and the characteristics and amount of the precipitated crystals. From the point of view of soil (specifically, uncemented soil), the effects of soil properties on G_0 have been extensively studied, including void ratio, confining pressure, particle size distribution (e.g. mean particle size D_{50} and coefficient of uniformity C_u which is defined as $\frac{D_{60}}{D_{10}}$). Empirical relationships were established to link the small-strain stiffness G_0 to void ratio, confining pressure and C_u [23, 45, 53, 63], as these variables are easy to access in the laboratory. Moreover, analytical and numerical studies revealed that the small-strain stiffness of a granular packing depends on the packing structure and particle properties. Theoretical models were developed based on these studies, such as the effective medium theory, to link the small-strain stiffness to the coordination number (or its variants) from a micromechanical perspective [1, 4, 34, 44].

Despite the fact that G_0 of soils with various properties have been widely studied, how various properties of soils affect the contribution of bio-cementation to G_0 remains to be explored. From the point of view of bio-cementation, the effects of the precipitated crystals with different characteristics on G_0 are not well studied. The characteristics of crystals include crystal polymorphism and distribution pattern. Specifically, calcium carbonate can precipitate in the form of different polymorphs (i.e. vaterite, aragonite or calcite) and metastable hydrated forms during MICP treatment [7]. In addition, the precipitated crystals can exhibit different distribution patterns in the pore space of the host soil [14, 32, 39, 60, 64, 74]. As conceptualised in Fig. 2, typical distribution patterns could be: bridging, which refers to carbonates located at the gap between sand grains and connects sand grains; contact cementing, representing those carbonate crystals that are located at contacts between sand particles; coating, referring to carbonates coating the sand grains; and pore filling, which represents carbonates filling in the void space and not bonding to sand grains. Note that, in the case of pore filling, carbonate particles are initially not in contact with

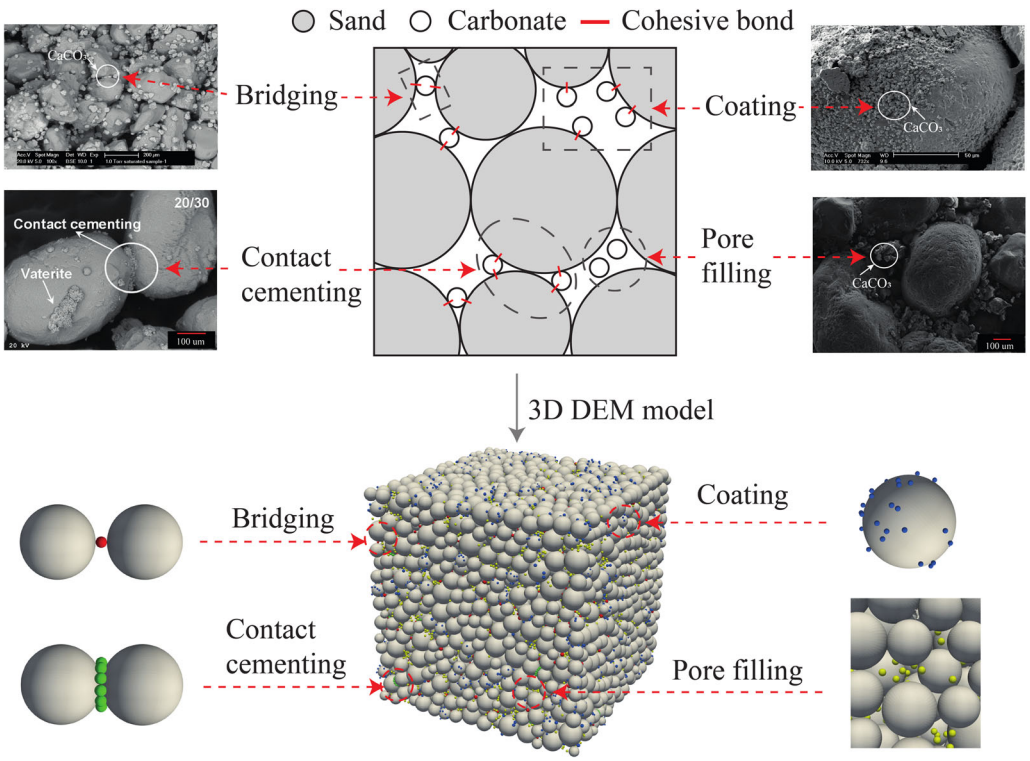

Fig. 2 Scanning electron microscopy (SEM) image, conceptualisation and DEM model example of bio-cemented soils with various distribution patterns of precipitated carbonates. SEM image illustrating bridging is from [46]; SEM image for contact cementing from [33]; SEM image for coating from [6] and the one for pore filling is from [65]

sand particles as gravity is not introduced in the present DEM simulations. Previous studies [73, 74] showed that different distribution patterns of crystals lead to significantly different impacts on the mechanical properties of bio-cemented sand. Therefore, to precisely describe the mechanical behaviour of bio-cemented soils, it is critical to identify not only the total amount of the precipitated crystals, but also the proportions of crystals of each distribution pattern. Understanding how seismic measurements provide information on the characteristics of crystal distribution patterns is thus of importance.

In order to reveal the mechanisms underlying the effect that particle size distribution, crystal content and property and distribution pattern have on the small-strain stiffness of bio-cemented sands, particle-scale modelling is essential. Therefore, the discrete element method (DEM) is used in this study to model bio-cemented sands. To account for various microscopic characteristics, the precipitated crystals are explicitly modelled at pre-defined locations. The DEM specimens are subjected to static probing (drained triaxial test at small strain) to assess the small-strain stiffness [18–20, 36, 42, 49, 50, 55]. Static probing is effective as reported by [5], who found that the wave velocity derived from static probing is the same as the long-wavelength wave velocity derived from dynamic probing (simulating propagation of elastic wave).

The content of this paper is organised as follows: Sect. 3 describes the DEM methodology in detail. Section 4 and Sect. 5 present the simulation results of the small-strain stiffness of bio-cemented soils with different characteristics and the underlying mechanisms gained from microscopic observations. Section 6 investigates the correlation between the small-strain stiffness and peak strength of bio-cemented specimens. Section 7 summarises the main conclusion of this study and discusses practical implementations for supporting shear wave velocity measurements to assess the mechanical efficiency and effectiveness of bio-mediated treatment.

3 Methodology

3.1 DEM specimen preparation

DEM simulations are performed using the open-source platform YADE [59]. Bio-cemented specimens are modelled in two steps: an uncemented specimen is generated as the host sand, before smaller spheres representing carbonate crystals are introduced. In order to prepare the uncemented specimen, a set of spherical particles is generated inside a cubic space confined by three pairs of rigid and frictionless walls. The reference particle size distribution

(PSD) shown in Fig. 3 is used throughout this study, unless otherwise stated (in Sect. 4.4). It has a coefficient of uniformity C_u = 1.4 and $D_{\max}/D_{\min}$ = 3.31. Mass scaling is introduced to improve computational efficiency [17]. The particles are not in contact with each other initially. The host sand specimen is compacted by controlling the three pairs of walls to move towards the centre of the cube. The compaction process is terminated once the confining pressure reaches 100 kPa. At that moment, the inter-particle friction angle is adjusted to reach a target void ratio e while keeping the confining pressure equal to 100 kPa. Unless otherwise stated, the target void ratio is 0.695. After generation of the uncemented specimen, carbonate particles are introduced into the host sand at predefined locations to obtain cemented specimens with specific distribution patterns and carbonate contents as illustrated in Fig. 2. Extending the approach presented by Evans et al. [16] and Khoubani et al. [28] to model contact cementation, Zhang and Dieudonné [74, 75] enabled the study of additional carbonate distribution patterns, namely grain bridging, grain coating, pore filling type, and their combinations. A detailed description of the modelling algorithm used in this study to introduce carbonate particles can be found in [75]. Note that, for computational reasons, the carbonate particles located at a given sand-sand contact (contact cementing pattern) are not connected to each other, contrary to the approach presented in [75]. In order to generate cemented samples with mixed carbonate distribution patterns, carbonate particles in each distribution pattern are generated separately inside the same host sample. The mass of carbonate particles in each distribution pattern is controlled to obtain the target mass ratio. After that, carbonate particles introduced at undesired locations (e.g. embedded within other particles) are removed. Finally, the generated cemented specimens are then subjected to static probing.

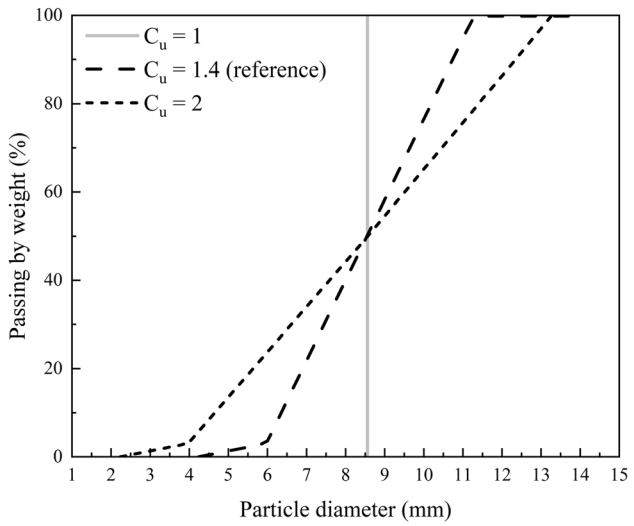

Fig. 3 Particle size distributions of the uncemented (host) sand

3.2 Contact model

The contact model used in this study is based on the classical linear elastic–plastic law from [10], with the introduction of cohesion. It is briefly introduced below. Details of this contact model can be found in [59].

For two spheres of radii R_1 and R_2 in contact, the normal force $\vec{F}_n$ and incremental shear force $\Delta\vec{F}_s$ are calculated as:

$$\vec{F}_n = k_n u_n \vec{n} \tag{1}$$

and

$$\Delta\vec{F}_s = -k_s \Delta\vec{u}_s \tag{2}$$

where u_n is the relative normal displacement of the two spheres, $\vec{n}$ is the normal contact vector and $\Delta\vec{u}_s$ is the incremental tangential displacement. k_n and k_s are the contact normal stiffness and tangential stiffness, respectively, which are given by:

$$k_n = \frac{2E_1R_1E_2R_2}{E_1R_1 + E_2R_2} \tag{3}$$

and

$$k_s = vk_n \tag{4}$$

where E_i $(i = 1, 2)$ is the modulus of elasticity of sphere i, and v is the shear stiffness coefficient. The normal and shear resistances are equal to:

$$F_n^{\max} = \sigma_{\text{coh}} \min(R_1, R_2)^2 \tag{5}$$

and

$$F_s^{\max} = \|\vec{F}_n\| \tan\varphi_c + \sigma_{\text{coh}} \min(R_1, R_2)^2 \tag{6}$$

where σ_{coh} is a cohesive strength parameter which controls the adhesion forces in the normal and tangential directions. φ_c is the contact friction angle. In this study, cohesion is only introduced at sand-carbonate contacts. The parameters of the sand and carbonate particles are indicated in Table 1.

Table 1 Properties of particles used in the static probing test

Parameter	Symbol	Unit	Sand	Carbonate
Density	ρ	kg/m^3	2650	2710
Young's modulus	E_s, E_c	GPa	1	1
Shear stiffness coefficient	v	–	0.3	0.3
Friction angle	φ_c	°	30	30
Cohesive strength	σ_{coh}	GPa	10	

3.3 Static probing test

3.3.1 Calculation of the shear modulus

After generation of the granular assemblies, a stress relaxation process is applied before the specimen is subjected to static probing. The stress relaxation process is applied until the unbalanced force ratio (defined as the ratio between the mean static unbalanced force and the mean contact force) is reduced below 1×10^{-8}, which ensures a quasi-static state [5, 18, 21, 55]. After the stress relaxation process, the probing test is conducted to calculate the shear modulus G. In the probing test, small-strain increments are applied in the axial direction while the lateral confining stress is maintained constant. G is calculated as:

$$G = \frac{\Delta q}{3\Delta\varepsilon_q} \tag{7}$$

where Δq is the increment of deviatoric stress and $\Delta\varepsilon_q = \Delta\varepsilon_1 - (\Delta\varepsilon_1 + \Delta\varepsilon_2 + \Delta\varepsilon_3)/3$ is the incremental deviatoric strain, with $\Delta\varepsilon_1$ the incremental axial strain, and $\Delta\varepsilon_2$ and $\Delta\varepsilon_3$, the two lateral strain increments.

3.3.2 Determination of the elastic regime

The maximum strain level ensuring that the DEM specimens remain within the elastic regime must be identified prior to determining the small-strain shear modulus. Therefore, static probing tests are run at different strain levels, and the corresponding shear modulus G is calculated for each strain level. Figure 4 presents the evolution of the calculated G with the strain level. The figure shows that the shear modulus remains approximately constant around $\varepsilon_q = 1 \times 10^{-6}$, before dropping with ε_q further increases. This conclusion aligns with findings from [31, 50], among others. Consequently, $\varepsilon_q = 1 \times 10^{-6}$ is selected as the reference state for calculating the small-strain shear stiffness G_0. This reference value of ε_q is also proved to be valid in the cases of cemented specimens (Fig. 6).

3.4 Determination of the REV size

The size of the representative elementary volume (REV) should be determined to ensure representativeness of the results. Five specimen sizes with 750, 1000, 2000, 3500 and 5000 sand particles, following the same particle size distribution, are considered. Six specimens are generated randomly for each specimen size.

Figure 5 shows that, for specimens with less than 3500 particles, the specimen size affects the average value of the small-strain stiffness, as well as the dispersion of the results. Smaller specimens exhibit on average a higher small-strain shear modulus than larger specimens, and the dispersion of the results is greater for small specimens. Consequently, a specimen containing 3500 sand particles is selected as the REV and used for the subsequent simulations.

4 Cemented specimens with a single carbonate distribution pattern

Bio-cemented specimens with a single carbonate distribution pattern, i.e. either bridging, contact cementing, coating or pore filling, are subjected to static probing under

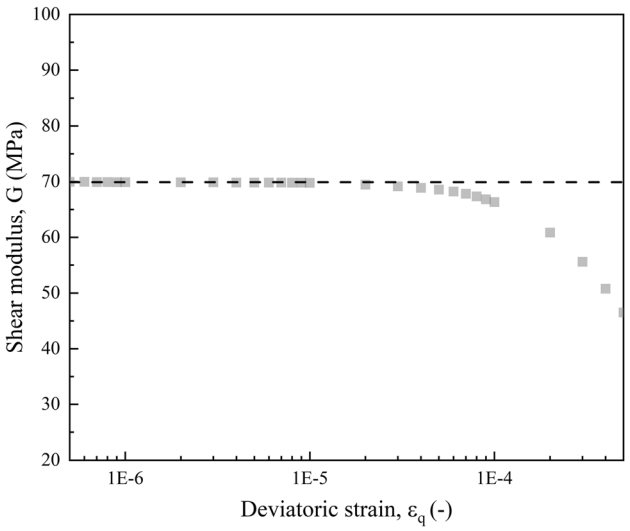

Fig. 4 Evolution of the shear modulus of the host sand with deviatoric strain

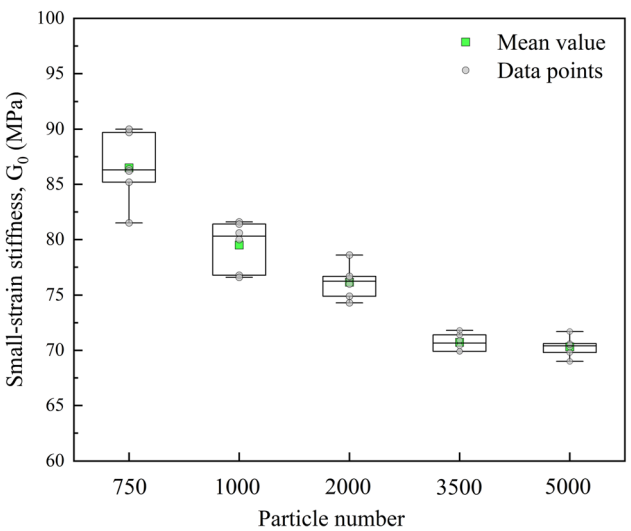

Fig. 5 Small-strain stiffness of specimens with various particle numbers

100 kPa confining pressure. The parameters of the sand and carbonate particles used in this study are presented in Table 1, unless otherwise stated. The cohesive strength parameter σ_{coh} is set to 10 GPa for sand-carbonate contacts, which is high enough to ensure that no bond breakage occurs within the elastic regime. The carbonate content is 1% for the cemented specimens unless otherwise stated in Sect. 4.3. Throughout this study, the carbonate content is defined as the dry mass of carbonate over the mass of the sand.

4.1 Carbonate distribution pattern

Fig. 6 presents the evolution of the shear modulus of cemented specimens with different carbonate distribution patterns as a function of the deviatoric strain. For all cemented specimens presented in Fig. 6, the shear modulus stays at a plateau around $\varepsilon_q = 1 \times 10^{-6}$. This suggests that the small-strain stiffness G_0 of cemented specimens can also be determined at a deviatoric strain $\varepsilon_q = 1 \times 10^{-6}$. For cemented specimens with other carbonate contents, a similar evolution of G with ε_q is observed. Consequently, $\varepsilon_q = 1 \times 10^{-6}$ is also selected as the state for calculating G_0 of cemented specimens.

Figure 6 further shows that the carbonate distribution pattern plays a critical role in G_0 of bio-cemented soils. For cemented specimens with 1% carbonate content, carbonate particles in the forms of bridging and contact cementing lead to obvious improvement in G_0. By contrast, carbonate particles distributed in the form of coating and pore filling show negligible difference compared to the uncemented specimen.

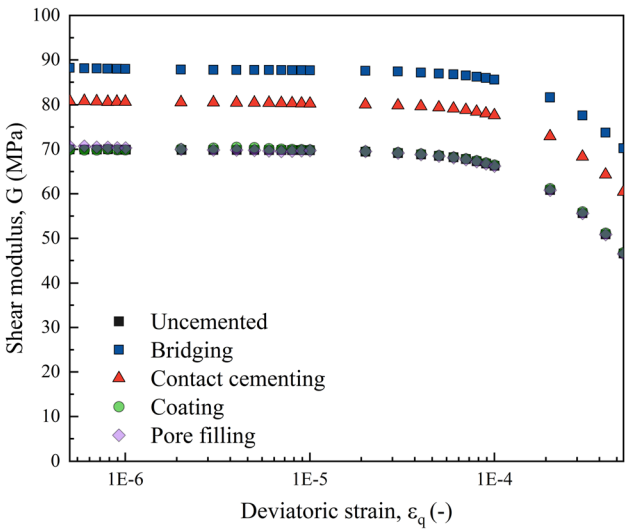

Fig. 6 Evolution of the shear modulus with deviatoric strain for bio-cemented specimens with different carbonate distribution patterns

4.2 Young's modulus of carbonate particles

Calcium carbonate ($CaCO_3$) has three polymorphs: vaterite, aragonite and calcite. During the treatment process of MICP or EICP, calcium carbonate can precipitate in any of the three polymorphs depending on the pH environment, temperature and the urea-$CaCl_2$ solution concentrations, among others. Clarà Saracho et al. [7] utilised XRD analysis to characterise $CaCO_3$ phase from MICP treatment with different ureolytic bacterial strains and found that different ureolytic bacterial strains can lead to different primary polymorphs of the precipitates. Al Qabany[46] and Paassen [2] reported that very high urease activities may result in the precipitation of vaterite initially. Mujah et al. [40] and Terzis et al. [57] observed a transformation of the precipitated crystals from vaterite to calcite as solutions were continuously injected during the treatment. In addition, metastable hydrated forms, including monohydrocalcite ($CaCO_3 \cdot H_2O$), ikaite ($CaCO_3 \cdot 6H_2O$), calcium carbonate hemihydrate ($CaCO_3 \cdot 1/2H_2O$), and amorphous calcium carbonate (ACC) can also exist [8, 58, 79]. Their estimated Young's modulus varies in a large range, from 25 to 91.28 GPa (see Table 2). By contrast, the Young's modulus of quartz sand is around 97 GPa [48]. To investigate the effect of the elastic properties of the precipitated crystal on the small-strain stiffness of bio-cemented soil, static probing tests are carried out on bio-cemented specimens with various ratios of sand and carbonate elastic moduli, E_s/E_c. Figure 7 illustrates the variation of G_0 with E_s/E_c, where E_s/E_c ranges from 0.1 to 10 by fixing E_s at 1 GPa while varying E_c. The carbonate content is 1% for all the cemented samples herein. The small-strain shear stiffness of the uncemented specimen is also included for reference. It can be found from Fig. 7 that:

Table 2 Literature review on the estimated Young's modulus of various carbonates and metastable hydrated carbonates

	Young's modulus (GPa)	Source
Calcite	77.6 to 96.8	[3, 15]
Vaterite	67.2 to 70	[15]
Aragonite	43 to 75	[76]
$CaCO_3 \cdot H_2O$	65.9 to 71.7	[3, 78]
$CaCO_3 \cdot 6H_2O$	41.9 to 66	[3, 78]
$CaCO_3 \cdot 1/2H_2O$	91.3	[78]
ACC	25 to 30	[30]

Note that several of the species are structurally anisotropic, and their elastic property exhibits a directional dependence. The range of the estimated Young's modulus for a given species partially reflects this anisotropy

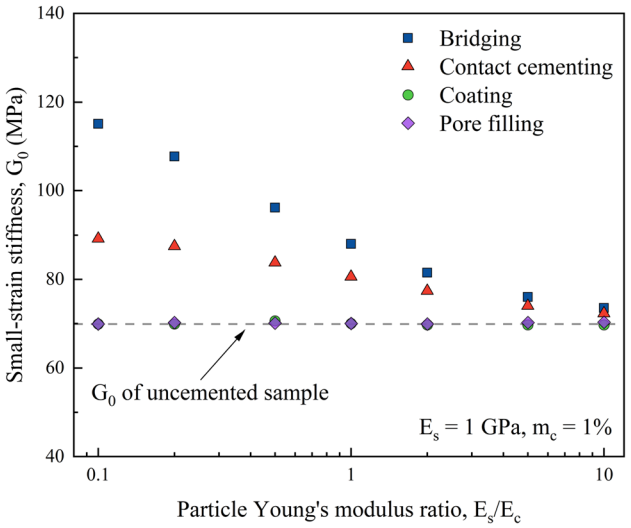

Fig. 7 Effect of sand-carbonate Young's modulus ratio (E_s/E_c) on the small-strain stiffness (G_0) of bio-cemented specimens

1. For all values of E_s/E_c, there is always an improvement in G_0 in the cases of bridging and contact cementing compared to uncemented specimen, even if E_c is lower than E_s. This suggests all the crystals, as long as in the pattern of bridging and contact cementing, have a positive effect on G_0.
2. The benefit of cementation in bridging and contact cementing pattern decreases with increasing E_s/E_c.
3. Crystals in the form of coating and pore filling do not lead to any increase in G_0, independently of E_s/E_c.

The reason why a lower E_c value leads to a lower improvement in G_0 in the cases of bridging and contact cementing is linked to the contact stiffness. According to Eq. (3) and (4), the stiffness of a sand-crystal contact increases with the increase of E_c when E_s is fixed. Therefore, the small-strain stiffness G_0 for both bridging and contact cementing shows a decreasing trend as E_s/E_c increases.

For a given E_s/E_c ratio, differences in the number of effective bonds explain that bridging cementation leads to higher improvement in G_0 than contact cementing, while coating and pore filling exhibit no improvement. Effective bonds refer to crystals which build connections between sand grains. Specifically, bridging holds more effective bonds than contact cementing at 1% of carbonate content. By contrast, there is no effective bond built in the cases of coating and pore filling. This can be supported by the effective coordination number (Z_e) proposed by [74]. The effective coordination number describes the average number of effective bonds per sand grain, in which only the contacts that contribute to the overall connections among sand grains are considered. It is defined as:

$$Z_e = \frac{2(C_s + C_b)}{N_s} \tag{8}$$

where N_s is the number of sand particles, C_s is the total number of sand–sand (S–S) contacts and C_b is the number of effective bond in cemented specimens. In the case of bridging, every carbonate connects two sand grains initially. Therefore, C_b is equal to the number of carbonate particles. In the case of contact cementing, several carbonates together strengthen one S–S contact. Therefore, in this case, C_b is equal to the number of S–S contacts which have been cemented. Finally, in the case of coating and pore filling, C_b is equal to zero as carbonate particles do not introduce connections between sand grains. In this way, the mechanical contribution of carbonate particles explicitly modelled and distributed following different distribution patterns can be well described. A detailed discussion on Z_e compared to traditional coordination number and mechanical coordination number can be found in [74].

For cemented specimens with m_c = 1%, bridging holds the largest Z_e which is 6.99, while the effective coordination number is equal to 5.03 for contact cementing, suggesting a higher improvement in G_0 in the case of bridging. The Z_e of specimens exhibiting coating and pore filling is 4.3, similarly to that of the uncemented specimen, corresponding to an absence of improvement in G_0 in these two cases.

4.3 Carbonate content

Figure 8a presents the evolution of the small-strain shear modulus with increasing carbonate content. Figure 8a shows that, for carbonate contents up to 3%, the small-strain stiffness of the material is not affected by carbonate crystals coating the sand particles or filling the pore space. On the other hand, bridging and contact cementing type of specimens exhibit obvious improvement in G_0 even with a small amount of carbonate content. In addition, the magnitude of improvement in G_0 increases with m_c for both bridging and contact cementing, which agrees with the findings reported by Ning et al. [43]. This can be attributed to the increase in the number of effective bonds (described by Z_e) with m_c, as shown in Fig. 8b. DEM cemented specimens with carbonate contents exceeding 3% are not covered in this study. The implementation of a more advanced model to introduce carbonate particles (e.g. considering irregular particle shape) is necessary to achieve high carbonate contents.

It should be noted that bridging always shows higher Z_e than contact cementing given the same m_c. However, the improvement in G_0 of bridging does not always outperform that of contact cementing. For instance, at m_c = 3%, bridging and contact cementing almost show the same

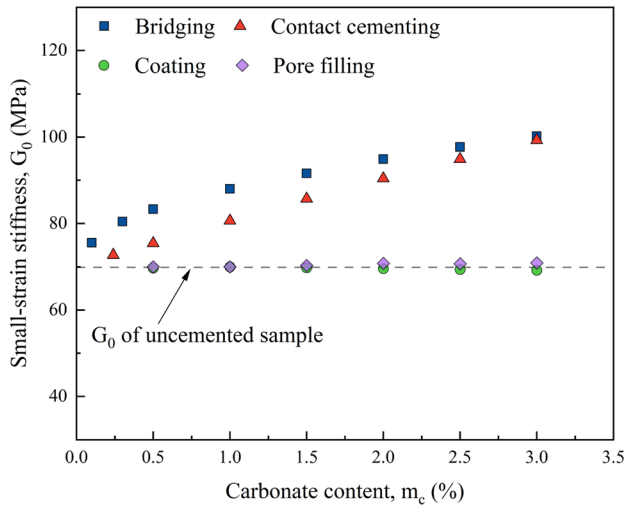

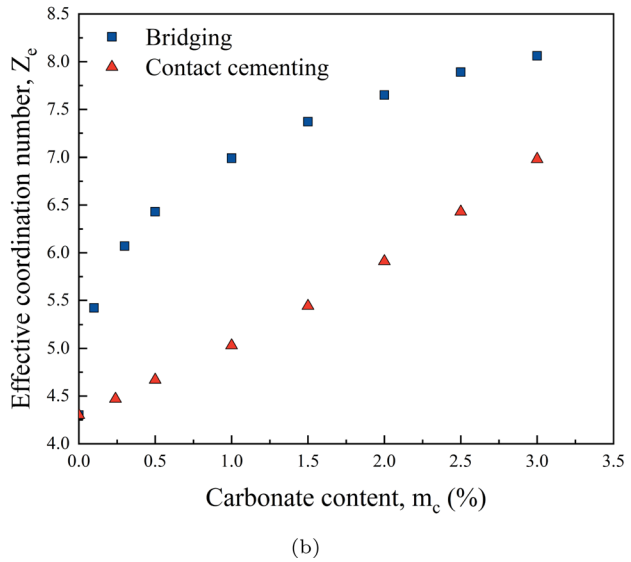

Fig. 8 Effect of carbonate content m_c on **a** the small-strain stiffness G_0 and **b** the effective coordination number Z_e

improvement in G_0, even though bridging holds more effective bonds than contact cementing. This suggests that the overall improvement in G_0 is not only related to the number of effective bonds. In fact, it is also related to the ability to improve stiffness from a single effective bond. To evaluate the contribution to stiffness from a single effective bond in the form of bridging and contact cementing, an axial loading test is carried out on two sand grains cemented with one effective bond in the form of contact cementing and bridging, respectively. The case of two sands without cementation is also tested as reference. The axial loading tests and the associated force–displacement relationship are shown in Fig. 9. It can be seen that the overall stiffness of contact cementing is 8.47×10^6 N/m, which reflects the stiffness of the sand–sand contact (which

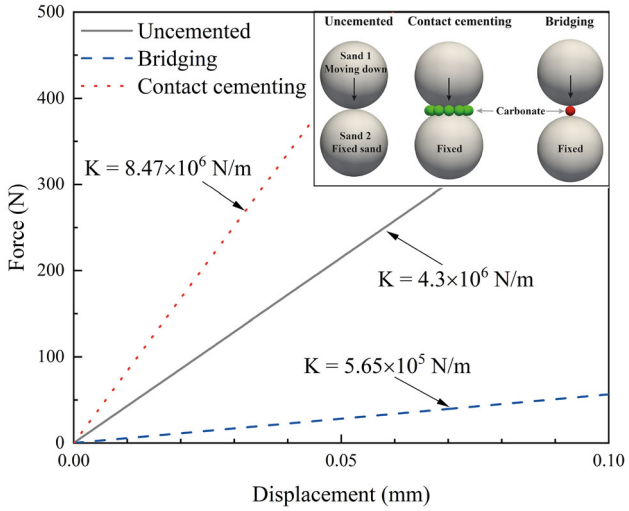

Fig. 9 Force–displacement results of axial loading tests on two sands without cementation and with cementation in the pattern of bridging and contact cementing, respectively

is 4.3×10^6 N/m) and the stiffness due to cementation. Accordingly, the net contribution of an effective bond in the contact cementing pattern to stiffness is 4.17×10^6 N/m, which is higher than the contribution of one effective bond in the bridging pattern (5.65×10^5 N/m).

Since one effective bond in the pattern of contact cementing can lead to more improvement in stiffness than one in bridging pattern, at a lower m_c, it is the number of effective bonds that dominates the improvement in overall stiffness. At this stage, bridging outperforms contact cementing because it shows higher Z_e. On the other hand, as the number of effective bonds increases with the increase of m_c, G_0 increases in both bridging and contact cementing cases but contact cementing benefits more from the increase of Z_e. Therefore, at a higher m_c, G_0 of bridging is almost the same as that of contact cementing even though bridging exhibits higher Z_e.

4.4 Host sand particle size distribution

The three particle size distributions of host sand specimen shown in Fig. 3 are considered. The particle size distributions have the same mean particle size D_{50} of 8.6 mm, but different C_u, namely C_u = 1 (monodisperse size distribution), C_u = 1.4 and C_u = 2. Host sand specimens with different C_u exhibit different G_0, which is 89.1 MPa for C_u = 169.9 MPa for C_u = 1.4 and 27.4 MPa for C_u = 2. This is consistent with the results from [25, 63] and [21], which concluded that the small-strain stiffness of sands is not influenced by the mean particle size, it decreases as the coefficient of uniformity of the soil increases. Since host sand specimens with different PSDs exhibit different G_0, a stiffness enhancement factor (SEF) is introduced to

describe the magnitude of improvement of G_0 on top of the corresponding host sand specimen. It is defined as:

$$\mathrm{SEF} = \frac{G_0^{cemented} - G_0^{uncemented}}{G_0^{uncemented}} \tag{9}$$

The stiffness enhancement factors of cemented specimens are compared in Fig. 10. Only bridging and contact cementing type of cemented specimens (m_c = 1%) are included in Fig. 10, as coating and pore filling type of specimens exhibit almost the same G_0 as that of corresponding host sand specimen. It can be seen from Fig. 10 that with a given PSD uniformity, the improvement in G_0 increases with carbonate content for both bridging and contact cementing cases. In addition, for the same carbonate content, the improvement in G_0 increases with C_u in both bridging and contact cementing. Moreover, the improvement in G_0 of bridging type exceeds that of contact cementing type in cases of C_u = 1 and C_u = 1.4, while this phenomenon is reversed for the cases of C_u = 2. This finding suggests that the desired carbonate distribution pattern which can most boost the improvement of small-strain stiffness depends on the PSD uniformity of the soils to be treated.

The underlying reason why the performance of contact cementing cases is more influenced by PSD uniformity than bridging cases can be attributed to the intrinsic properties of the host sand. Two intrinsic properties are considered, specifically, the number of sand–sand (S–S) contacts (as carbonates are deployed at S–S contacts in contact cementing cases), and the gap size distribution (since carbonates are located at grain gaps for bridging pattern), as illustrated in Fig. 2. Host specimens with the same initial void ratio, particle number and confining pressure show different average numbers of S–S contacts given different PSD uniformity. The change in C_u leads to an obvious change in the number of sand-sand contacts, which can be supported by the coordination number of S–S contacts Z_{SS} (defined as the average number of S–S contacts per sand grain). As shown in Fig. 11, Z_{SS} is 5.07 for host sand with C_u = 1, 4.3 for host sand with C_u = 1.4 and 2.19 for host sand with C_u = 2, suggesting that the number of sand–sand contacts is largely affected by PSD uniformity and therefore the deployment of carbonates in contact cementing pattern. By contrast, the change of C_u does not result in an obvious difference in the gap size distribution in the range under consideration, as shown in Fig. 12, which suggests that the deployment of carbonates in bridging pattern is not sensitive to the change of C_u.

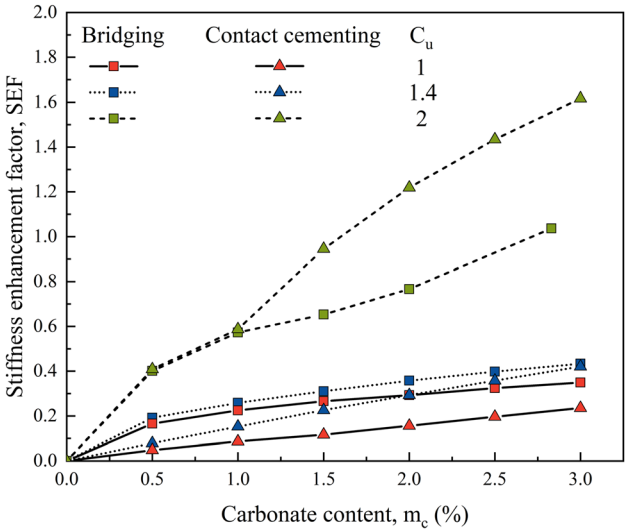

Fig. 10 The small-strain stiffness enhancement factor (SEF) of cemented specimens with different distribution patterns and carbonate content (m_c) generated from host specimens with various PSD uniformity (C_u)

4.5 Host sand void ratio

Figure 13a presents the stiffness enhancement factors of cemented specimens with m_c = 1% prepared from host sand specimens with various void ratios. Only bridging and contact cementing type of specimens with m_c = 1% are included in Fig. 13a. It can be seen that:

1. The stiffness enhancement factor increases with increasing void ratio in both bridging and contact cementing cases. The reason can be attributed to the fact that the host specimen holds fewer S–S contacts with an increasing void ratio (i.e. a decreasing trend in Z_e shown in Fig. 13b). The ratio of the number of effective bonds to the number of S–S contacts increases, as shown in Fig. 13b, suggesting that the

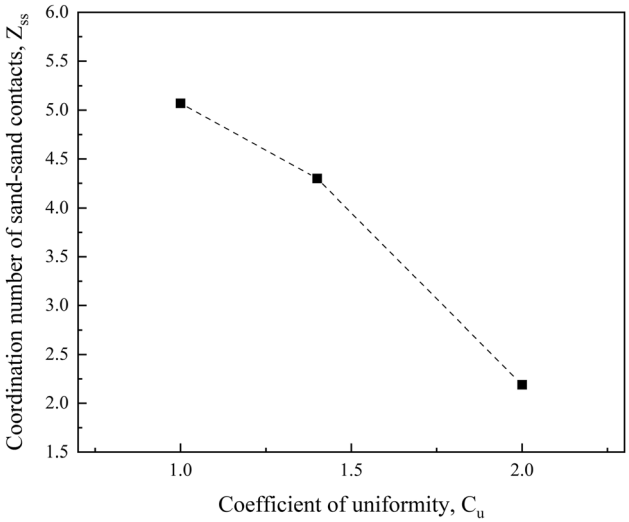

Fig. 11 Effect of PSD uniformity on the coordination number of sand-sand contacts (Z_{SS})

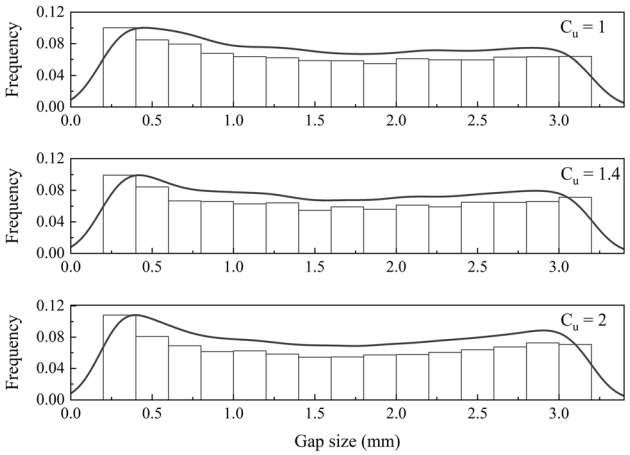

Fig. 12 Effect of PSD uniformity on the gap size distribution of host sand specimens

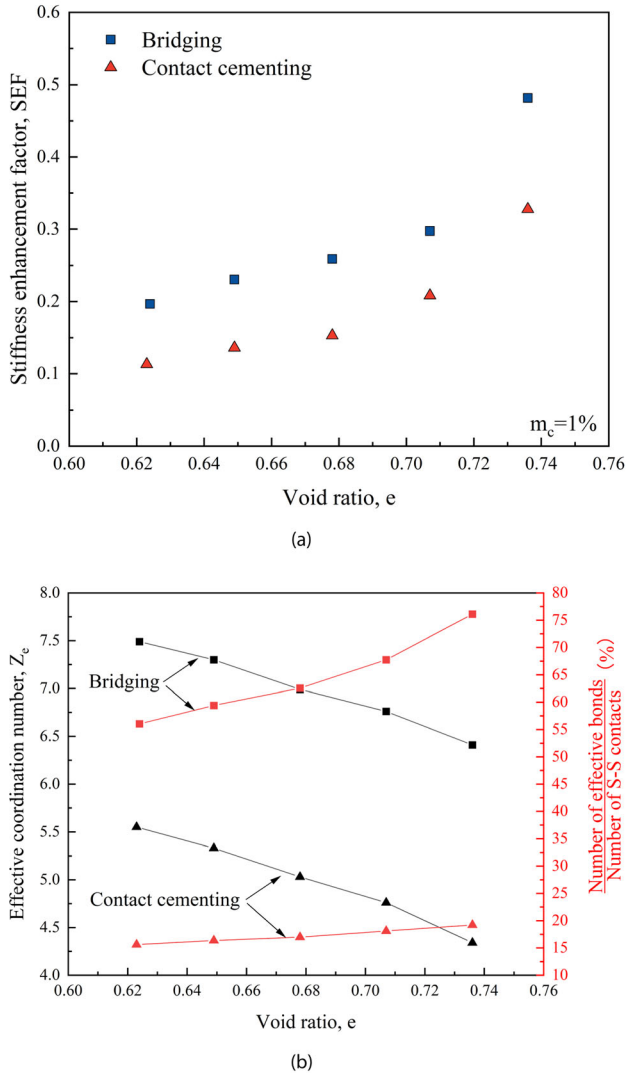

Fig. 13 Effect of initial void ratio of host sand on **a** small-strain stiffness enhancement factor (SEF), **b** Z_e and ratio of number of effective bonds/ number of S–S contacts

effective bonds are taking the dominating role with the increasing void ratio.

2. Bridging always shows a larger improvement in G_0 compared to that of the corresponding contact cementing specimen, independent of the void ratio of the host sand specimen. This can be attributed to the fact that for the cases of m_c = 1% in which the number of effective bonds that dominates the improvement in overall stiffness as discussed before, there are more effective bonds (i.e. higher Z_e) in bridging specimens compared to contact cementing ones, as presented in Fig. 13b.

5 Cemented specimens with mixed carbonate distribution patterns

In reality, bio-cemented specimens usually exhibit mixed distribution patterns. As discussed in the above analysis, not all the precipitated carbonates can contribute to improvements in G_0: carbonates precipitated in the pattern of coating and pore filling hardly contribute to the improvement in G_0, and thus they are regarded as non-effective precipitation. Moreover, carbonates distributed in the form of bridging and contact cementing lead to improvements but with different levels, given the same amount of precipitation. In this section, cemented specimens with mixed distribution patterns are generated based on the host sand specimen with C_u = 1.4 and an initial void ratio of 0.695. The specimens are subjected to a static probing test at 100 kPa of confinement. As carbonates precipitated in the pattern of coating and pore filling are non-effective precipitation. Thereby, three components are considered in mixed distribution patterns: bridging, contact cementing and non-effective precipitation. Note that non-effective precipitation is represented by carbonate in coating pattern to account for the carbonate mass in that part. Fifteen cemented specimens are generated, and each of the specimens contains 2% of carbonates and has specific mass ratios among the three distribution patterns, as demonstrated by a ternary plot shown in Fig. 14. For instance, S1-B0C0N1, S11-B1C0N0 and S15-B0C1N0 represent the cemented specimen with a single carbonate distribution pattern, i.e. pure coating, bridging and contact cementing type of specimen with 2% of carbonates, respectively. Specimen S5-B1C1N2 contains 2% of carbonates in which the mass ratio of carbonates in the pattern of bridging, contact cementing and non-effective (coating) is 1:1:2.

Figure 15 shows the contour of the stiffness enhancement factor. It can be seen that, for the same amount of carbonate content, bio-cemented specimens can exhibit

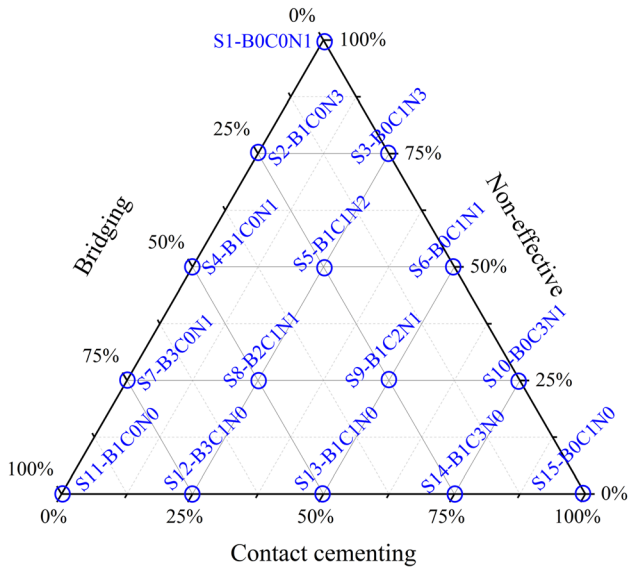

Fig. 14 Ternary plot illustrating bio-cemented specimens with mixed distribution patterns. Sampling points are marked by circles. The name of each specimen indicates its ID and mass ratio of carbonates in the pattern of bridging (B) versus contact cementing (C) versus non-effective (N)

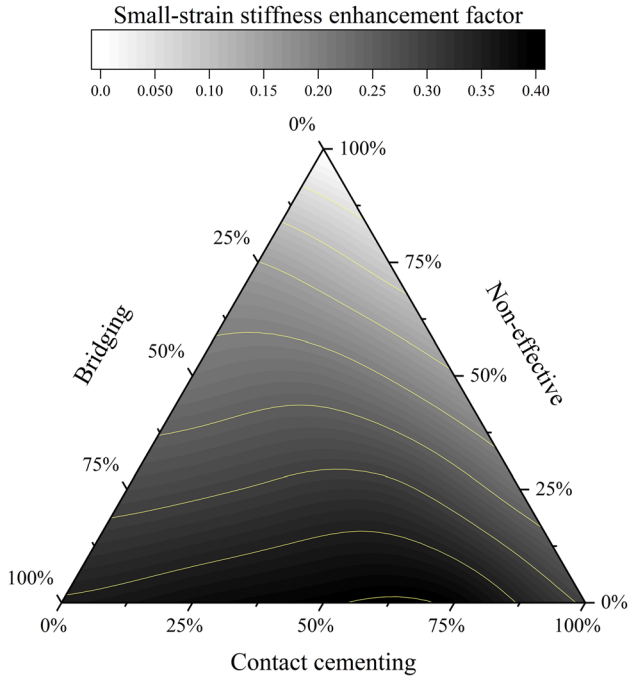

Fig. 15 Contour of the small-strain stiffness enhancement factor for bio-cemented soils with mixed $CaCO_3$ distribution patterns

different levels of improvement in G_0, highly depending on the relative proportions of carbonates of each distribution pattern. It is also interesting to note that for bio-cemented specimens with a single carbonate distribution pattern, bridging one (S11-B1C0N0) exhibits the largest stiffness enhancement factor compared to S1-B0C0N1 and S15-B0C1N0. While bio-cemented specimens whose carbonates precipitate in a combination form of bridging and contact cementing pattern tend to show even greater improvement in G_0, for instance, S14-B1C3N0 shows the highest stiffness enhancement factor among all the specimens. This can be understood as for pure bridging one (S11-B1C1N0), the number of effective bonds may be maximised but the overall improvement in G_0 may not be optimal as one effective bond in the pattern of bridging shows less contribution than one in contact cementing. On the other hand, for pure contact cementing one (S15-B0C1N0), the overall improvement may not be optimal as the number of effective bonds is relatively small, given the same m_c. Thereby, a combination of bridging and contact cementing which balances the number of effective bonds and the contribution ability can lead to the most improvement in G_0.

6 Correlation between G_0 and peak strength

To investigate the relationship between the small-strain stiffness and peak strength, 18 cemented specimens (bridging and contact cementing only) with different carbonate contents and C_u are selected from specimens used in Sect. 4.4 and subjected to drained triaxial compression tests under 100 kPa of confining pressure in DEM. A detailed description of drained triaxial compression simulation can be found in [74]. The contact friction angle (φ_c) used in the triaxial compression simulations is 30° which is the same as that used for the static probing tests. The cohesive strength parameter (σ_{coh}) for sand-carbonate contacts is set as 10MPa initially. The peak strength obtained from the stress–strain curve of the triaxial

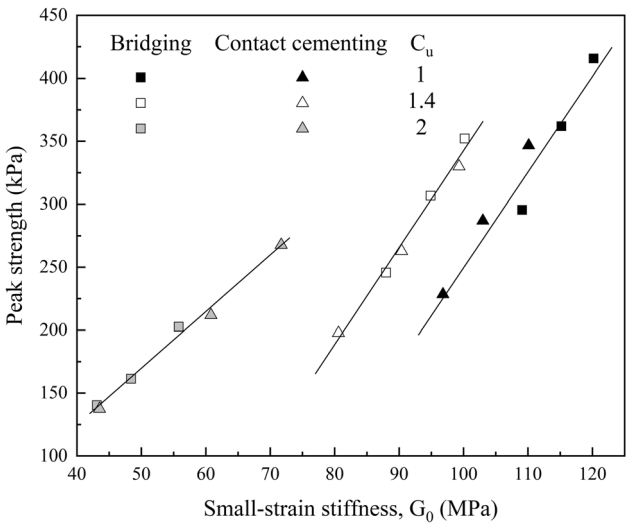

Fig. 16 Correlation between small-strain stiffness and peak strength

compression test is plotted against the small-strain stiffness as shown in Fig. 16. It can be seen that, for both bridging and contact cementing type of cemented specimens, the small-strain stiffness shows a linear relationship with the peak strength in all the C_u cases presented in Fig. 16. This suggests that small-strain stiffness is a good indicator of soil strength, supporting the approach of using geophysical measurements to monitor and map the strength of treated soils. The strategy that uses the shear wave velocity or small-strain stiffness to estimate the peak strength is further supported by experimental findings from [54, 70], who also found a correlation between the small-strain stiffness and the peak strength of weakly cemented soils and granular soils, respectively.

7 Discussion and conclusions

The significant uncertainty associated with bio-mediated treatment poses a central challenge, limiting the practical implementation of such methods. Enhancing confidence in treatment outcomes can be achieved through non-destructive means, such as employing seismic measurement techniques, both in laboratory and field settings. The shear wave velocity can be derived from seismic measurements and used as a key indicator of the treatment effect. This study contributes to the fundamental understanding of how bio-cementation affects the small-strain stiffness, hence the shear wave velocity, of bio-cemented sands. Therefore, it aims to support seismic measurement as a means to assess the mechanical efficiency and effectiveness of bio-mediated treatment.

The results of this study indicate that the characteristics of bio-cementation affect the improvement in G_0. The main findings are summarised as follows:

1. The carbonate distribution pattern plays an important role in the effectiveness of bio-cementation. Specifically, grain coating and pore filling hardly affect G_0, hence are regarded as non-effective precipitation from a mechanical point of view. By contrast, grain bridging and contact cementing emerge as precipitation patterns that lead to significant improvement in G_0. Beneficial treatment is associated with effective connections of sand grains (which can be described by the effective coordination number). This finding indicates that seismic methods are useful to assess the performance of the treatment, as compared to carbonate content measurements, which do not provide insight into the microscopic distribution of the minerals.
2. Calcium carbonate crystals precipitated in the pattern of bridging and contact cementing can lead to an increase in G_0, regardless of whether their Young's modulus is higher or lower than that of sand grains. On the other hand, crystals with different Young's moduli exhibit different efficiencies in improvement in G_0: those with a higher Young's modulus lead to higher improvement in G_0. From this perspective, the mechanism that dominates the mechanical efficiency of bio-cementation is the contact stiffness of particle-to-particle contacts. This supports that the measured shear wave velocity or small-strain stiffness can reflect the mechanical efficiency of bio-cementation.
3. The properties of the host sand, specifically the void ratio and coefficient of uniformity of the particle size distribution, affect the response of bio-cementation on improvement in the small-strain stiffness of bio-cemented sands. With varying void ratios and coefficient of uniformity, the number of sand-sand contacts, which provide sites for contact cementing, as well as the gap size distribution, which provides sites for grain bridging, change but with different magnitudes. This leads to different mechanical responses to contact cementing and bridging cementation. In this case, two mechanisms determine together the overall mechanical efficiency of bio-cementation: the number of effective bonds and the ability of a single bond to stiffness improvement.

Overall, the small-strain stiffness of bio-cemented soil is not only related to the characteristics (e.g. polymorph and distribution pattern) of the precipitated crystals but also varies with the host soil. On the one hand, different characteristics of the precipitated crystals contribute differently to the improvement in the small-strain stiffness of bio-cemented soils. On the other hand, different soils respond differently given the same amount and characteristic of the precipitated crystals. This finding extends what has been found in [74], which reported that the bridging pattern is the optimal distribution pattern as it leads to the most strength improvement. In fact, there is no optimal distribution pattern of carbonate that is universally applicable to all types of soils. Moreover, the small-strain stiffness shows a linear relationship with the peak strength. These findings support the use of seismic measurement to probe the overall performance of bio-mediated treatment. Finally, four carbonate distribution patterns are investigated in this paper. However, more complex carbonate distribution patterns can exist in bio-cemented soils. For instance, carbonate crystals can connect to multiple soil grains simultaneously. Modelling this complex carbonate distribution pattern requires the implementation of non-spherical particle shapes in the DEM model. Approaches such as clumps [11, 55] and level set DEM [26, 27] can be adopted to this end.

Acknowledgements The first author acknowledges support from the China Scholarship Council (CSC) and the Geo-Engineering Section of Delft University of Technology, The Netherlands.

Author contribution Conceptualization: A.Z., A.C.D.; Methodology: A.Z., A.C.D., V.M., H.C.; Formal analysis and investigation: A.Z.; Writing - original draft preparation: A.Z.; Writing - review and editing: all authors; Funding acquisition: A.Z., A.C.D., T.H.; Supervision: A.C.D., T.H.

Declarations

Conflict of interest The authors declare no competing interests.

References

1. Agnolin I, Roux JN (2007) Internal states of model isotropic granular packings. iii. Elastic properties. Phys Rev E 76(6):061–304
2. Al Qabany AAA (2011) Microbial carbonate precipitation in soils. PhD thesis, University of Cambridge
3. Chahi G, Bradai D, Belabbas I (2020) Structural and elastic properties of $CaCO_3$ hydrated phases: a dispersion-corrected density functional theory study. J Phys Chem Solids 138(109):295
4. Chang CS, Misra A, Sundaram SS (1991) Properties of granular packings under low amplitude cyclic loading. Soil Dyn Earthq Eng 10(4):201–211
5. Cheng H, Luding S, Saitoh K et al (2020) Elastic wave propagation in dry granular media: effects of probing characteristics and stress history. Int J Solids Struct 187:85–99
6. Cheng L, Shahin MA, Mujah D (2016) Influence of key environmental conditions on microbially induced cementation for soil stabilization. J Geotech Geoenviron Eng 143(1):08304016
7. Clarà Saracho A, Haigh SK, Hata T et al (2020) Characterisation of $CaCO_3$ phases during strain-specific ureolytic precipitation. Sci Rep 10(1):1–12
8. Clarà Saracho A, Lucherini L, Hirsch M et al (2021) Controlling the calcium carbonate microstructure of engineered living building materials. J Mater Chem A 9(43):24438–24451
9. Cui MJ, Lai HJ, Hoang T et al (2021) One-phase-low-PH enzyme induced carbonate precipitation (EICP) method for soil improvement. Acta Geotech 16:481–489
10. Cundall PA, Strack OD (1979) A discrete numerical model for granular assemblies. Géotechnique 29(1):47–65
11. Dai BB, Li TQ, Deng LJ et al (2022) Fabric effect on the angle of repose in granular materials. Powder Technol 400(117):256
12. Darby KM, Hernandez GL, DeJong JT et al (2019) Centrifuge model testing of liquefaction mitigation via microbially induced calcite precipitation. J Geotech Geoenviron Eng 145(10):04019084
13. DeJong JT, Fritzges MB, Nüsslein K (2006) Microbially induced cementation to control sand response to undrained shear. J Geotech Geoenviron Eng 132(11):1381–1392
14. DeJong JT, Mortensen BM, Martinez BC et al (2010) Bio-mediated soil improvement. Ecol Eng 36(2):197–210
15. Ekprasert J, Fongkaew I, Chainakun P et al (2020) Investigating mechanical properties and biocement application of $CaCO_3$ precipitated by a newly-isolated *Lysinibacillus* sp. WH using artificial neural networks. Sci Rep 10(1):1–13
16. Evans T, Khoubani A, Montoya B (2014) Simulating mechanical response in bio-cemented sands. In: Computer methods and recent advances in geomechanics: proceedings of the 14th international conference of international association for computer methods and recent advances in geomechanics, Taylor & Francis Books Ltd, pp 1569–1574
17. Feng K, Montoya B, Evans T (2017) Discrete element method simulations of bio-cemented sands. Comput Geotech 85:139–150
18. Gong J, Wang X, Li L et al (2019) DEM study of the effect of fines content on the small-strain stiffness of gap-graded soils. Comput Geotech 112:35–40
19. Gu X, Yang S (2018) Why the OCR may reduce the small strain shear stiffness of granular materials? Acta Geotech 13(6):1467–1472
20. Gu X, Yang J, Huang M (2013) DEM simulations of the small strain stiffness of granular soils: effect of stress ratio. Granul Matter 15(3):287–298
21. Gu X, Lu L, Qian J (2017) Discrete element modeling of the effect of particle size distribution on the small strain stiffness of granular soils. Particuology 32:21–29
22. Hamdan N, Kavazanjian E Jr (2016) Enzyme-induced carbonate mineral precipitation for fugitive dust control. Géotechnique 66(7):546–555
23. Hardin BO, Richart F Jr (1963) Elastic wave velocities in granular soils. J Soil Mech Found Div 89(1):33–65
24. Ivanov V, Chu J (2008) Applications of microorganisms to geotechnical engineering for bioclogging and biocementation of soil in situ. Rev Environ Sci Bio/Technol 7(2):139–153
25. Iwasaki T, Tatsuoka F (1977) Effects of grain size and grading on dynamic shear moduli of sands. Soils Found 17(3):19–35
26. Kawamoto R, Andò E, Viggiani G et al (2016) Level set discrete element method for three-dimensional computations with triaxial case study. J Mech Phys Solids 91:1–13
27. Kawamoto R, Andò E, Viggiani G et al (2018) All you need is shape: Predicting shear banding in sand with LS-DEM. J Mech Phys Solids 111:375–392
28. Khoubani A, Evans T, Montoya B (2016) Particulate simulations of triaxial tests on bio-cemented sand using a new cementation model. Geo-Chicago 2016:84–93
29. Krishnan V, Khodadadi Tirkolaei H, Martin K et al (2021) Variability in the unconfined compressive strength of EICP-treated"standard" sand. J Geotech Geoenviron Eng 147(4):06021001
30. Lee SW, Kim YJ, Lee YH et al (2016) Behavior and characteristics of amorphous calcium carbonate and calcite using $CaCO_3$ film synthesis. Mater Des 112:367–373

31. Likitlersuang S, Teachavorasinskun S, Surarak C et al (2013) Small strain stiffness and stiffness degradation curve of Bangkok clays. Soils Found 53(4):498–509
32. Lin H, Suleiman MT, Brown DG et al (2015) Mechanical behavior of sands treated by microbially induced carbonate precipitation. J Geotech Geoenviron Eng 142(2):04015066
33. Lin H, Suleiman MT, Brown DG et al (2016) Mechanical behavior of sands treated by microbially induced carbonate precipitation. J Geotech Geoenviron Eng 142(2):04015066
34. Liu D, Morimoto T, Carraro JAH et al (2022) A semi-empirical re-evaluation of the influence of state on elastic stiffness in granular materials. Granul Matter 24(2):56
35. Ma G, Xiao Y, Fan W et al (2022) Mechanical properties of biocement formed by microbially induced carbonate precipitation. Acta Geotech 17(11):4905–4919
36. Magnanimo V, La Ragione L, Jenkins JT et al (2008) Characterizing the shear and bulk moduli of an idealized granular material. EPL (Europhys Lett) 81(3):34006
37. Mitchell JK, Santamarina JC (2005) Biological considerations in geotechnical engineering. J Geotech Geoenviron Eng 131(10):1222–1233
38. Montoya BM, Do J, Gabr MA (2021) Distribution and properties of microbially induced carbonate precipitation in underwater sand bed. J Geotech Geoenviron Eng 147(10):04021098
39. Mujah D, Shahin MA, Cheng L (2017) State-of-the-art review of biocementation by microbially induced calcite precipitation (MICP) for soil stabilization. Geomicrobiol J 34(6):524–537
40. Mujah D, Cheng L, Shahin MA (2019) Microstructural and geomechanical study on biocemented sand for optimization of MICP process. J Mater Civ Eng 31(4):04019025
41. Nafisi A, Montoya BM, Evans TM (2020) Shear strength envelopes of biocemented sands with varying particle size and cementation level. J Geotech Geoenviron Eng 146(3):04020002
42. Nie JY, Shi XS, Cui YF et al (2022) Numerical evaluation of particle shape effect on small strain properties of granular soils. Eng Geol 303(106):652
43. Ning Z, Khoubani A, Evans T (2017) Particulate modeling of cementation effects on small and large strain behaviors in granular material. Granul Matter 19(1):7
44. Otsubo M, Kuwano R, O'Sullivan C et al (2022) Using geophysical data to quantify stress transmission in gap-graded granular materials. Géotechnique 72(7):565–582
45. Oztoprak S, Bolton M (2013) Stiffness of sands through a laboratory test database. Géotechnique 63(1):54–70
46. van Paassen LA (2009) Biogrout, ground improvement by microbial induced carbonate precipitation. PhD thesis, Delft University of Technology
47. van Paassen LA, Ghose R, van der Linden TJ et al (2010) Quantifying biomediated ground improvement by ureolysis: large-scale biogrout experiment. J Geotech Geoenviron Eng 136(12):1721–1728
48. Peng Z, Redfern SA (2013) Mechanical properties of quartz at the α-β phase transition: Implications for tectonic and seismic anomalies. Geochem Geophys Geosyst 14(1):18–28
49. Perez JL, Kwok C, Senetakis K (2016) Effect of rubber size on the behaviour of sand-rubber mixtures: a numerical investigation. Comput Geotech 80:199–214
50. Reddy NS, He H, Senetakis K (2022) DEM analysis of small and small-to-medium strain shear modulus of sands. Comput Geotech 141(104):518
51. Rinaldi V, Santamarina J (2008) Cemented soils: small strain stiffness. Deform Charact Geomater 1(1):267–273
52. Riveros GA, Sadrekarimi A (2020) Effect of microbially induced cementation on the instability and critical state behaviours of fraser river sand. Can Geotech J 57(12):1870–1880
53. Senetakis K, Madhusudhan B (2015) Dynamics of potential fill-backfill material at very small strains. Soils Found 55(5):1196–1210
54. Sharma R, Baxter C, Jander M (2011) Relationship between shear wave velocity and stresses at failure for weakly cemented sands during drained triaxial compression. Soils Found 51(4):761–771
55. Shi X, Nie J, Zhao J et al (2020) A homogenization equation for the small strain stiffness of gap-graded granular materials. Comput Geotech 121(103):440
56. Terzis D, Laloui L (2018) 3-D micro-architecture and mechanical response of soil cemented via microbial-induced calcite precipitation. Sci Rep 8(1):1416
57. Terzis D, Bernier-Latmani R, Laloui L (2016) Fabric characteristics and mechanical response of bio-improved sand to various treatment conditions. Geotech Lett 6(1):50–57
58. Tlili M, Amor MB, Gabrielli C et al (2002) Characterization of $CaCO_3$ hydrates by micro-Raman spectroscopy. J Raman Spectrosc 33(1):10–16
59. Šmilauer V, et al (2015) Yade Documentation 2nd ed. The Yade Project, https://doi.org/10.5281/zenodo.34073, http://yade-dem.org/doc/
60. Wang Y, Konstantinou C, Soga K et al (2022) Use of microfluidic experiments to optimize MICP treatment protocols for effective strength enhancement of MICP-treated sandy soils. Acta Geotech 17(9):3817–3838
61. Weil MH, DeJong JT, Martinez BC et al (2012) Seismic and resistivity measurements for real-time monitoring of microbially induced calcite precipitation in sand. Geotech Test J 35(2):330–341
62. Whiffin VS, van Paassen LA, Harkes MP (2007) Microbial carbonate precipitation as a soil improvement technique. Geomicrobiol J 24(5):417–423
63. Wichtmann T, Triantafyllidis T et al (2009) Influence of the grain-size distribution curve of quartz sand on the small strain shear modulus gmax. J Geotech Geoenviron Eng 135(10):1404
64. Wu H, Wu W, Liang W et al (2023) 3D DEM modeling of biocemented sand with fines as cementing agents. Int J Numer Anal Methods Geomech 47(2):212–240
65. Wu S, Li B, Chu J (2021) Stress-dilatancy behavior of MICP-treated sand. Int J Geomech 21(3):04020264
66. Xiao P, Liu H, Xiao Y et al (2018) Liquefaction resistance of biocemented calcareous sand. Soil Dyn Earthq Eng 107:9–19
67. Xiao Y, Wang Y, Wang S et al (2021) Homogeneity and mechanical behaviors of sands improved by a temperature-controlled one-phase MICP method. Acta Geotech 16(5):1417–1427
68. Xiao Y, Zhao C, Sun Y et al (2021) Compression behavior of MICP-treated sand with various gradations. Acta Geotech 16(5):1391–1400
69. Xiao Y, He X, Zaman M et al (2022) Review of strength improvements of biocemented soils. Int J Geomech 22(11):03122001
70. Yoo JK, Park D, Baxter CD (2018) Estimation of drained shear strength of granular soil from shear wave velocity and confining stress. J Geotech Geoenviron Eng 144(6):04018027
71. Zeng C, Veenis Y, Hall CA et al (2021) Experimental and numerical analysis of a field trial application of microbially induced calcite precipitation for ground stabilization. J Geotech Geoenviron Eng 147(7):05021003

72. Zeng C, van Paassen LA, Jj Zheng et al (2022) Soil stabilization with microbially induced desaturation and precipitation (MIDP) by denitrification: a field study. Acta Geotech 17(12):5359–5374
73. Zhang A, Dieudonné AC (2023a) Effects of carbonate distribution inhomogeneity on the improvement level of bio-cemented sands: A DEM study. In: International conference of the international association for computer methods and advances in geomechanics, Springer, pp 554–561
74. Zhang A, Dieudonné AC (2023) Effects of carbonate distribution pattern on the mechanical behaviour of bio-cemented sands: A DEM study. Comput Geotech 154(105):152
75. Zhang A, Dieudonné AC (2024) Cementor: a toolbox to generate bio-cemented soils with specific microstructures. Biogeotechnics 2:100081
76. Zhang N, Yang S, Xiong L et al (2016) Nanoscale toughening mechanism of nacre tablet. J Mech Behav Biomed Mater 53:200–209
77. Zhang X, Chen Y, Liu H et al (2020) Performance evaluation of a MICP-treated calcareous sandy foundation using shake table tests. Soil Dyn Earthq Eng 129(105):959
78. Zhou Y, Liu Q, Hu M et al (2020) Investigation on the stability, electronic, optical, and mechanical properties of novel calcium carbonate hydrates via first-principles calculations. Int J Quantum Chem 120(10):e26219
79. Zou Z, Habraken WJ, Matveeva G et al (2019) A hydrated crystalline calcium carbonate phase: calcium carbonate hemihydrate. Science 363(6425):396–400